Science Advances
AAAS

advances.sciencemag.org/cgi/content/full/5/7/eaav9186/DC1

Supplementary Materials for

Covalent chemistry on nanostructured substrates enables noninvasive quantification of gene rearrangements in circulating tumor cells

Jiantong Dong, Yu Jen Jan, Ju Cheng, Ryan Y. Zhang, Meng Meng, Matthew Smalley, Pin-Jung Chen, Xinghong Tang, Patrick Tseng, Lirong Bao, Tzu-Yang Huang, Dongjing Zhou, Yupin Liu, Xiaoshu Chai, Haibo Zhang, Anqi Zhou, Vatche G. Agopian, Edwin M. Posadas, Jing-Jong Shyue, Steven J. Jonas, Paul S. Weiss, Mengyuan Li*, Guangjuan Zheng*, Hsiao-hua Yu*, Meiping Zhao*, Hsian-Rong Tseng*, Yazhen Zhu*

*Corresponding author. Email: hrtseng@mednet.ucla.edu (H.-R.T.); yazhenzhu@mednet.ucla.edu (Y.Z.); mpzhao@pku.edu.cn (M.Z.); bruceyu@gate.sinica.edu.tw (H.-h.Y.); zhengguangjuan@163.com (G.Z.); mengyuanli@pku.edu.cn (M.L.)

Published 31 July 2019, *Sci. Adv.* **5**, eaav9186 (2019)
DOI: 10.1126/sciadv.aav9186

This PDF file includes:

1. High-resolution X-ray photoelectron spectroscopy characterization

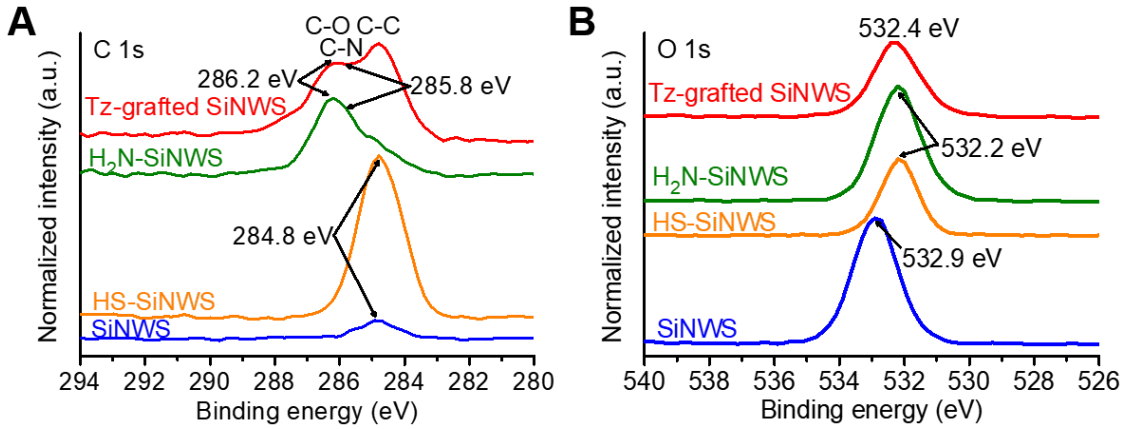

Fig. S1. High-resolution XPS characterization. High-resolution X-ray photoelectron spectroscopy (HR-XPS) spectra for silicon nanowire substrates (SiNWS), thiol-grafted SiNWS (HS-SiNWS), amine-grafted SiNWS (H_2N-SiNWS) and tetrazine-grafted SiNWS (Tz-grafted SiNWS) in the energy range of (**A**) C 1s signals; (**B**) O 1s signals.

As shown in fig. S1A, the high-resolution C 1s (284.8 eV) peak increased in intensity following silanization of the silicon nanowire substrates (SiNWS) to yield HS-SiNWS, which was consistent with the incorporation of C–C bonds at the SiNWS surface from the (3-mercaptopropyl)trimethoxysilane (MPS) silane. For H_2N-SiNWS, new peaks appeared at 285.8 and 286.2 eV corresponding to the C–N and C–O bonds, respectively, introduced by surface modification with OPSS-PEG-NH_2. The higher peak intensity observed at 285.8 eV for the tetrazine (Tz)-grafted SiNWS compared to the H_2N-SiNWS is suggestive of the increased number of C–N bonds introduced to the surface by the Tz motif. In fig. S1B, the O 1s peak shifted from 532.9 eV for SiNWS to 532.2 eV for HS-SiNWS and H_2N-SiNWS and then to 532.4 eV for the Tz-grafted SiNWS, which reflects the difference in O electronic states within the local bonding environment of the modified SiNWS.

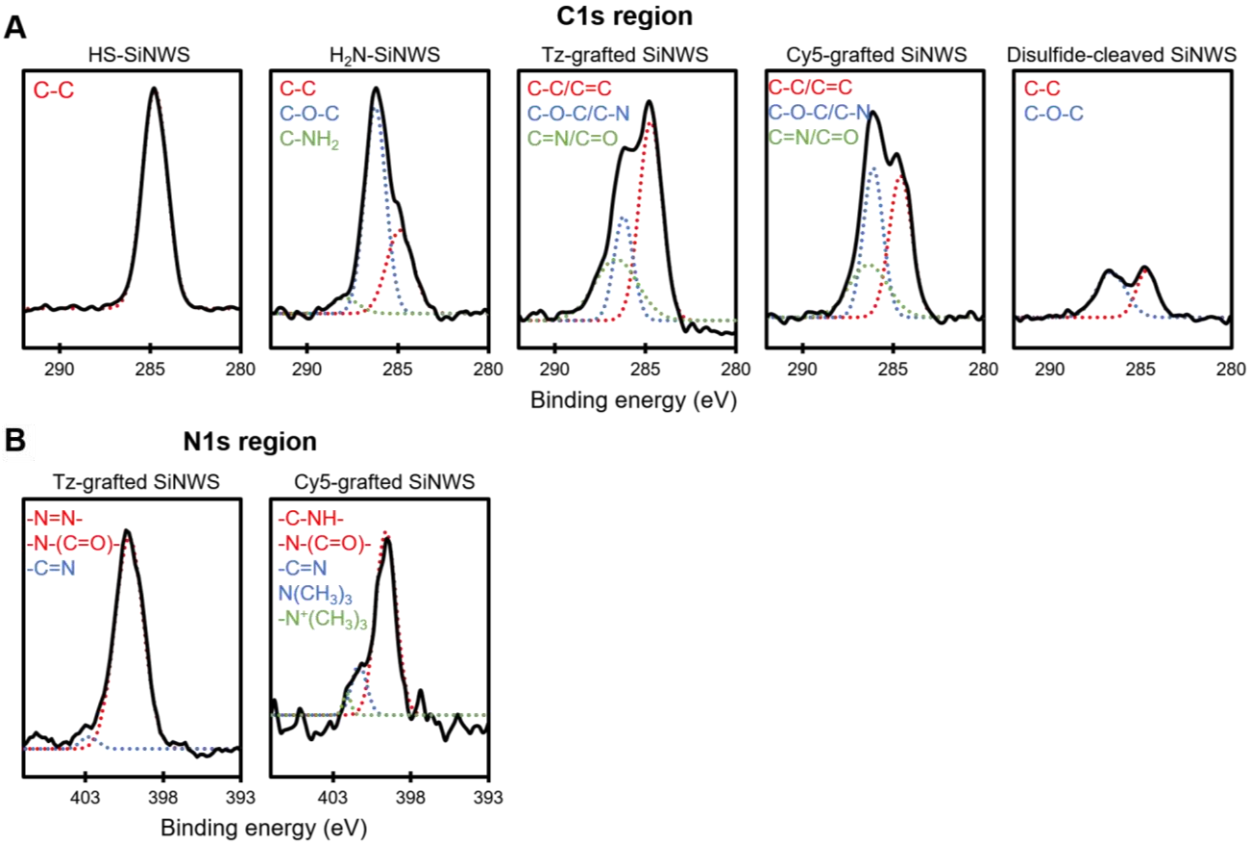

Fig. S2. Deconvolution of x-ray photoelectron spectra of stepwise functionalized SiNWS. (**A**) C1s and (**B**) N1s regions.

As demonstrated in the C1s deconvoluted spectra, C–C bond at 284.8 eV was observed after surface silation to form HS-SiNWS. Additional peaks of C–NH_2 bond at 288.0 eV and C–O–C bond at 286.4 eV was observed upon the formation of H_2N-SiNWS by reacting with OPSS-PEG-NH_2. Once the Tz groups were introduced, C=O/C=N bond at 286.7 eV appeared, identifying the successful conjugation of Tz groups. Upon the cleavage of the disulfide bond, only peaks corresponding to C–C and C–O–C bonds were observed, confirming the successful dissociation. Deconvolution of the peaks at the N1s region confirmed Cy5 labeling. Only N=N, N–(C=O) and -C=N peaks were observed on Tz-grafted SiNWS. Upon the introduction of Cy5, new peaks at 402.0 and 400.0 eV confirmed the cyanine structure of Cy5. Analysis of deconvoluted X-ray photoelectron spectra confirmed the bonding structure on the surface of SiNWS.

2. Fluorescence imaging for exploring bioorthogonal ligation

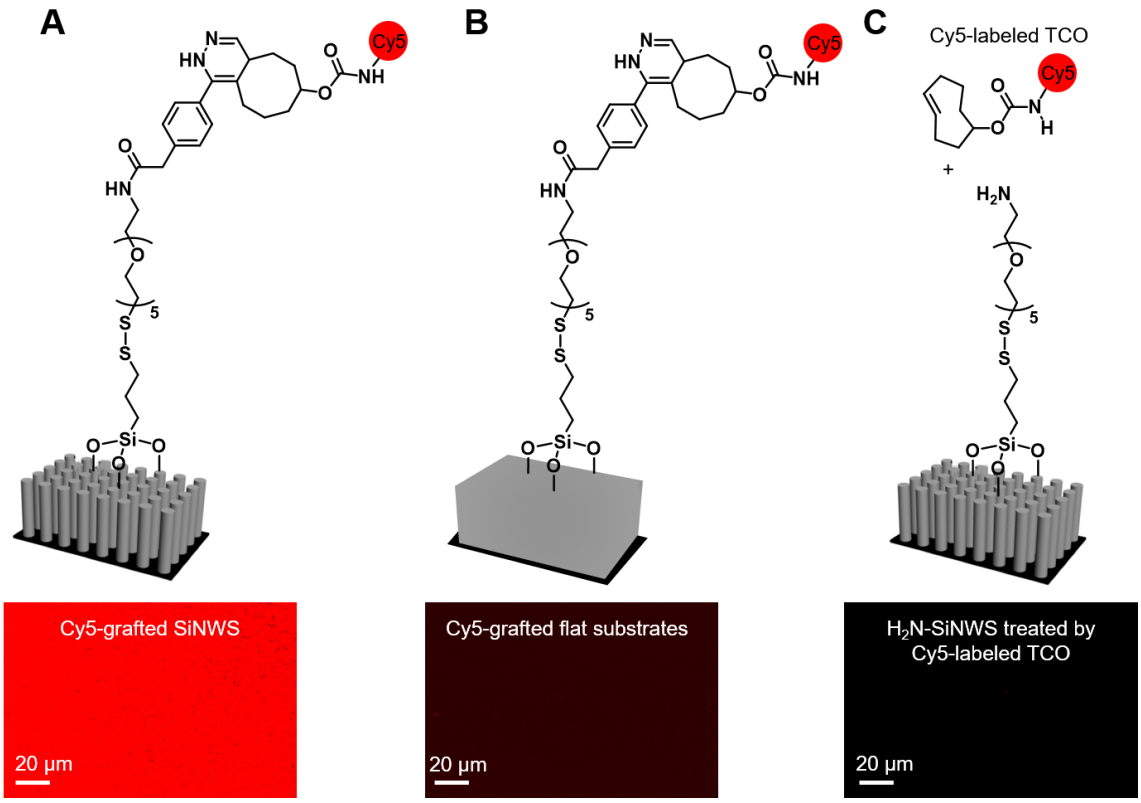

Fig. S3. Fluorescence imaging for exploring bioorthogonal ligation. Scheme and representative fluorescence images illustrating the bioorthogonal ligation of Cy5-labeled TCO to (**A**) Tz-grafted SiNWS, (**B**) Tz-grafted flat Si substrates and (**C**) H_2N-SiNWS.

3. Dynamic changes of Cy5 fluorescence intensity upon disulfide cleavage by 1,4-dithiothreitol

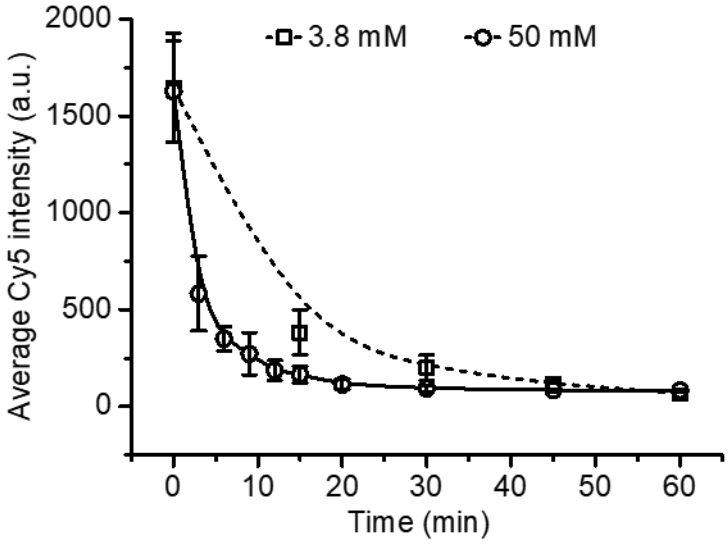

Fig. S4. Dynamic changes of Cy5 fluorescence intensity upon disulfide cleavage by DTT. Average Cy5 intensity vs. DTT reaction time on Cy5-grafted SiNWS with 3.8 mM (square and short dash line) and 50 mM (circle and solid line) DTT, respectively (n=8). The Cy5-grafted SiNWS were treated with DTT (3.8 mM) in PBS (200 µL) for 0, 15, 30, 45, and 60 min and DTT (50 mM) in PBS (200 µL) for 0, 3, 6, 9, 12, 15, 20, 30, 45, and 60 min, respectively.

The curves in fig. S3 indicate the fluorescence intensity of the Cy5 fluorophore decreased more rapidly after the exposure to 50 mM 1,4-dithiothreitol (DTT) for 3 min and plateaued between 60~80 a.u. within 12 min. This demonstrated that DTT can efficiently and quickly cleave the disulfide linkers present on the SiNWS, allowing release of captured biomolecules and/or cells.

4. Scheme of circulating tumor cell capture on tetrazine-grafted magnetic beads

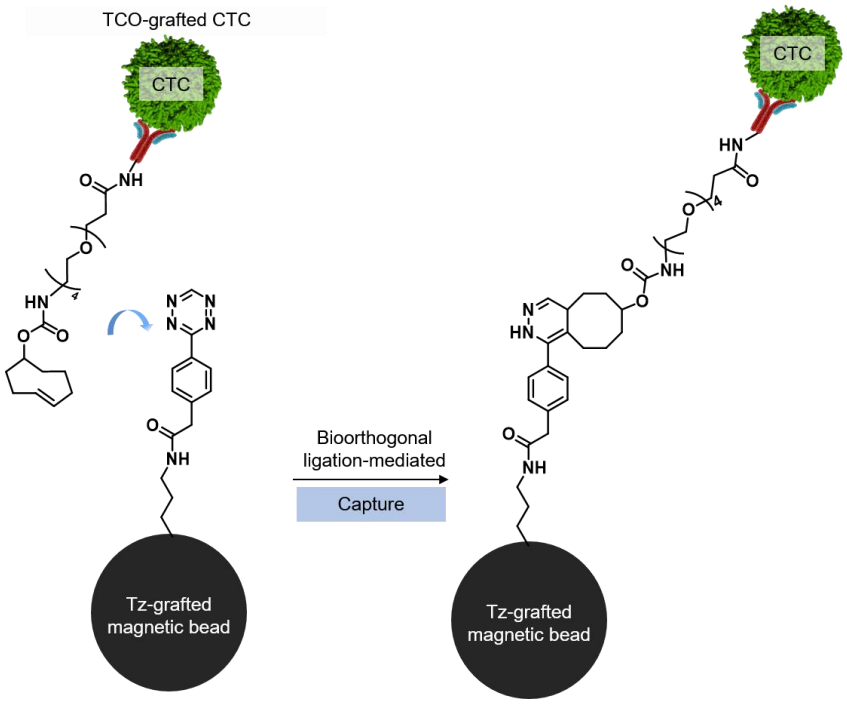

Fig. S5. Scheme of CTC capture on Tz-grafted magnetic beads.

To compare the capture performance of Click Chips with magnetic beads, we carried out bioorthogonal ligation-mediated CTC capture on Tz-grafted magnetic beads using pre-stained artificial CTC samples and a small quantity of 0.1-ng TCO-anti-EpCAM per capture study (the same quantity used with Click Chips). For each capture study, the Dynabeads™ M-270 Amine (2×10^8 beads, 100 µL, Thermo Fisher Scientific) were reacted with Tz-sulfo-NHS ester (0.32 mg, 3.8 mM) in PBS buffer for 1 h to produce the Tz-grated magnetic beads. The Tz-grafted magnetic beads were incubated with the TCO-grafted CTC samples at room temperature for 30 min. The CTC-captured magnetic beads were stained with DAPI and imaged under the fluorescence microscope (Nikon 90i).

5. Scheme of RT-ddPCR analysis of ALK/ROS1 rearrangements in circulating tumor cells

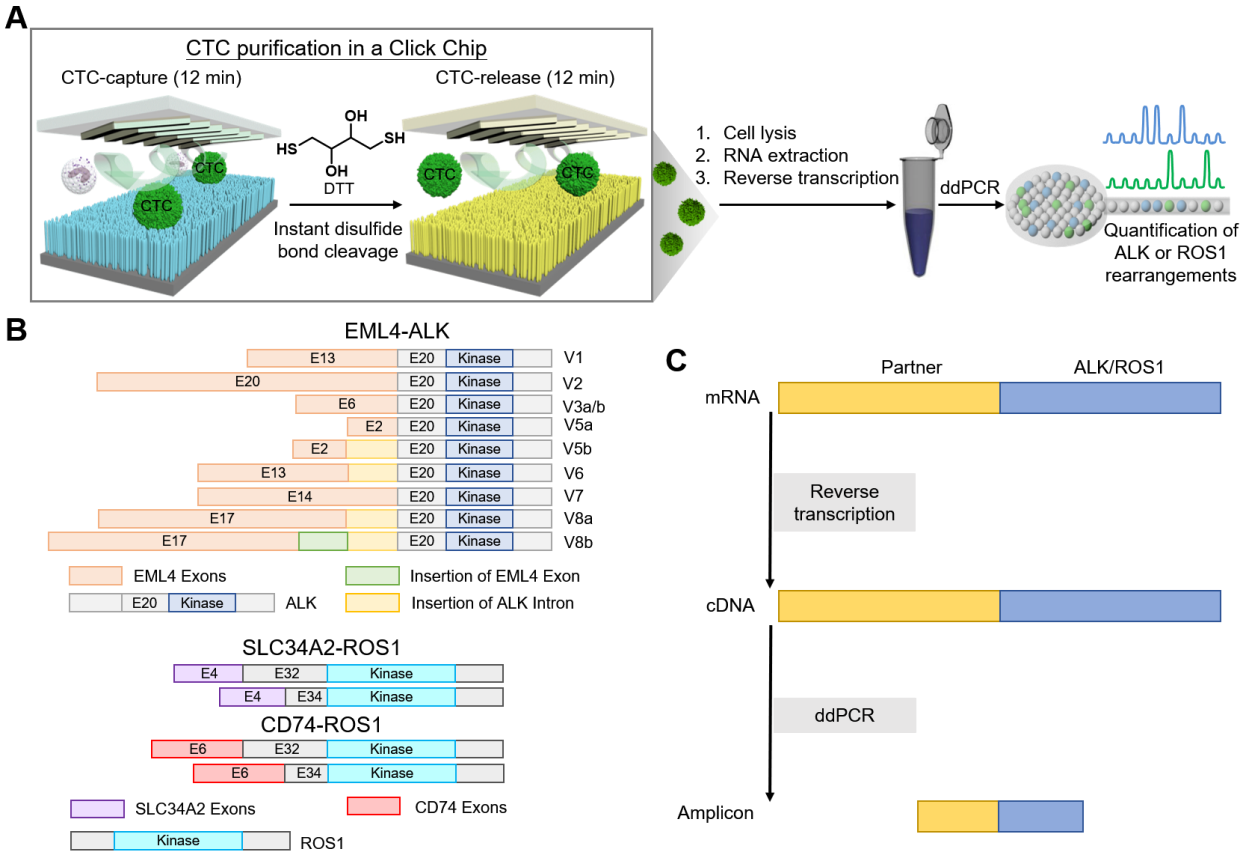

Fig. S6. Scheme of RT-ddPCR analysis of ALK/ROS1 rearrangements in CTCs. (**A**) The general workflow of the RT-ddPCR analysis of ALK/ROS1 rearrangements in CTCs coupled with CTC purification in Click Chips. (**B**) Schematic of the variants of the EML4-ALK rearrangement in H2228 cell line and non-small cell lung cancer (NSCLC) patients, the SLC34A2-ROS1 rearrangement in HCC78 cell line and CD74-ROS1 rearrangement in NSCLC patients. Different colors represent different domains. (**C**) Schematic depicting the workflow used for RT-ddPCR analysis of ALK/ROS1 rearrangements.

6. Dynamic ranges for RT-ddPCR quantification of ALK/ROS1 rearrangements

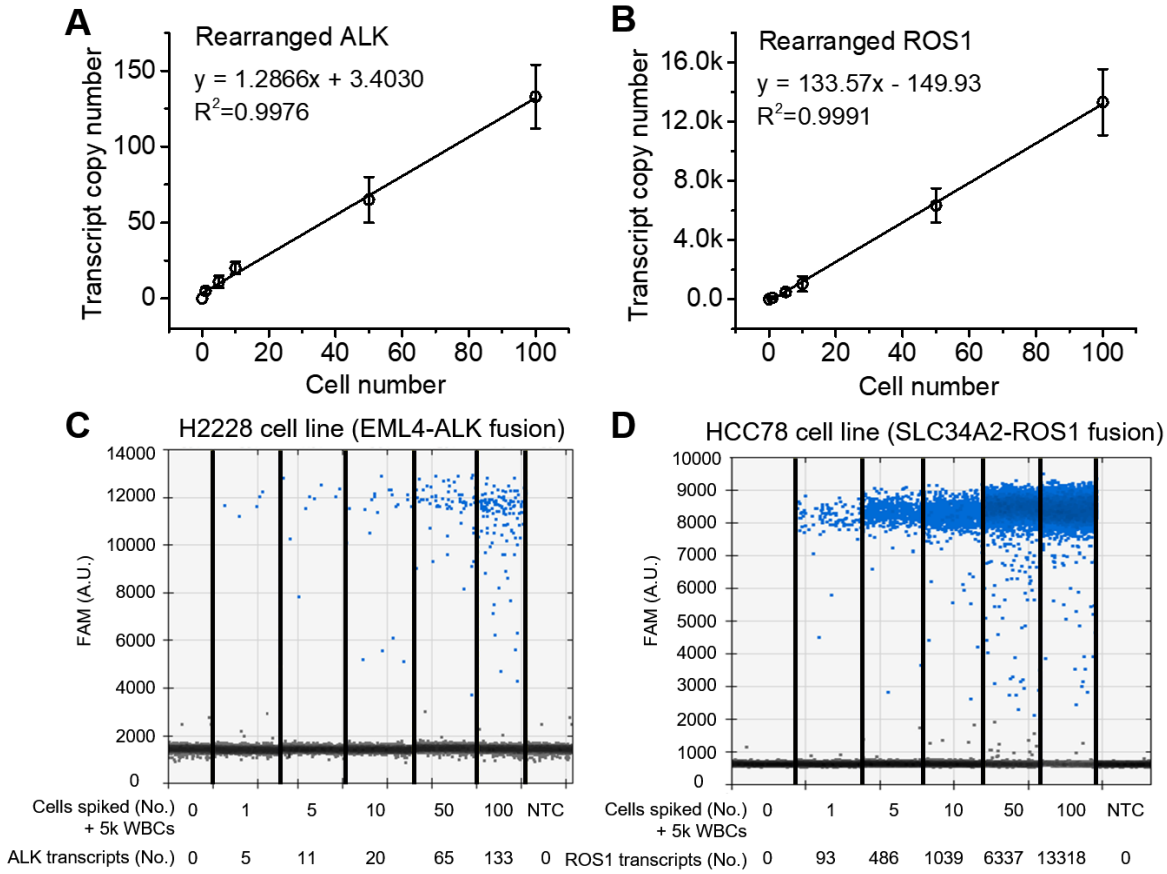

Fig. S7. Dynamic ranges for RT-ddPCR quantification of ALK/ROS1 rearrangements. Dynamic ranges for RT-ddPCR analysis of ALK/ROS1 rearrangements in a series of artificial CTC samples with a given number of CTCs: 0, 1, 5, 10, 50, 100 in suspensions of 5,000 WBCs. Non-template control (NTC) groups were also performed. (**A**) RT-ddPCR analysis of EML4-ALK rearrangement in artificial H2228 cell line samples. Regression analysis shows a linear correlation between the transcript copy number and the spiked number of H2228 cells. (**B**) RT-ddPCR analysis of SLC34A2-ROS1 rearrangement in artificial HCC78 cell line samples. Regression analysis indicates a linear correlation between the transcript copy number and the number of HCC78 cells in the artificial CTC sample. (**C**) Representative original 1-D plots for RT-ddPCR quantification of EML4-ALK rearrangements with each droplet from a sample plotted on the graph of fluorescence intensity *vs*. droplet number. (**D**) Representative original 1-D plots for RT-ddPCR quantification of SLC34A2-ROS1 rearrangements with each droplet from a sample plotted on the graph of fluorescence intensity *vs*. droplet number. For both (**C**) and (**D**), 6 samples (spiked with different numbers of cancer cells) were combined to generate one combined image for one experiment.

7. Comparison of cell lysis on-chip with cell lysis of 1,4-dithiothreitol-released cells

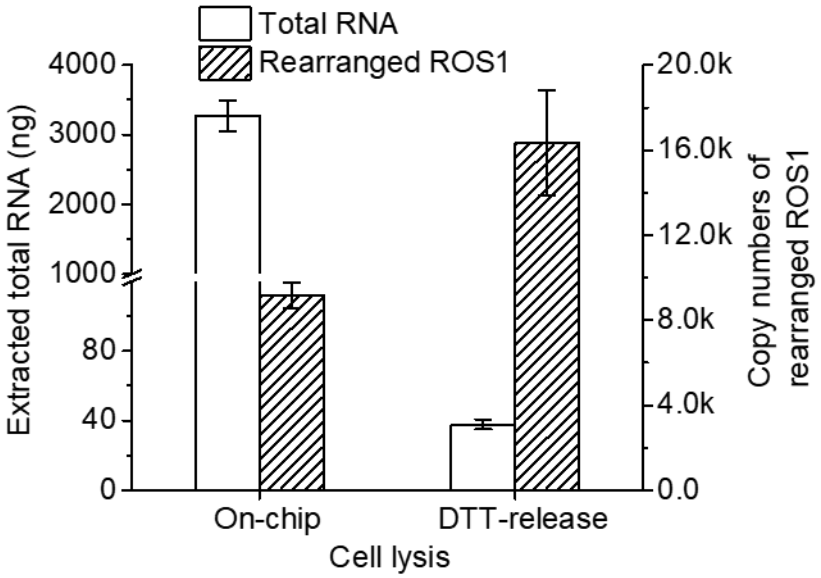

Fig. S8. Comparison of cell lysis on-chip with cell lysis of DTT-released cells. Comparison of cell lysis on-chip with cell lysis of 1,4-dithiothreitol (DTT)-released cells using artificial CTC samples by spiking 200 HCC78 cells into freshly purified human WBCs (5×10^6 cells mL^{-1}) in Roswell Park Memorial Institute (RPMI) medium (200 µL) on Click Chips (n=3).

We compared RNA products recovered following disulfide cleavage-mediated CTC release with samples where lysis was performed directly on Click Chips. After CTC capture using 200-µL artificial CTC samples, we injected TRI Reagent (1:3, (v/v), 600 µL) and ethanol (100%, 600 µL) sequentially into the Click Chips and collected the effluent liquid containing RNA in a 1.5 mL RNase-free Eppendorf tube. Then RNA purification was performed according to the standard procedure for the Direct-zol™ RNA MicroPrep Kit. The total extracted RNA was quantified using a NanoDrop™ 2000/2000c Spectrophotometer. The copy numbers of ROS1 rearrangement were quantified by RT-ddPCR procedures. As shown in fig. S7, even though on-chip lysis obtained a much larger amount of total RNA (>3000 ng) than what was obtained from DTT-released cell lysis products (<40 ng), the copy number of rearranged ROS1 (~9000 copies) was much lower than that of the DTT-released cell lysis samples (>16,000 copies). These results demonstrate the advantage of DTT-released cell lysis over on-chip lysis for improving the quantity and quality of target rearrangements collected.

Table S1. CTC purity during capture and release processes.

Experiment number	Bioorthogonal ligation-mediated capture		Disulfide cleavage-driven release	
	CTC number	WBC number	CTC number	WBC number
1	186	1682	148	152
2	185	1407	145	168
3	178	1050	133	147
4	177	2352	140	315
5	184	2121	159	252